Atmospherically resistant vegetation water indices using the 970-nm water absorption feature

Quanjun Jiao,[a] Liangyun Liu,[a,]* Jiangui Liu,[b] Hao Zhang,[a] and Bing Zhang[a]

[a]Chinese Academy of Sciences, Aerospace Information Research Institute,
Key Laboratory of Digital Earth Science, Beijing, China

[b]Agriculture and Agri-Food Canada, Ottawa, Ontario, Canada

Abstract. Atmospheric correction can introduce errors in surface spectral reflectance, and hence induces errors in plant water estimation from remote sensing water indices. We intend to develop water indices that are less impacted by atmospheric effects for plant water content estimation based on the 970-nm water absorption feature. A simulation study using the PROSAIL and 6S models showed that uncertainty in atmospheric water vapor (WV) content can induce large variation in existing 970-nm water indices, such as WI, NWI-1, and NWI-3. An attempt was made to incorporate atmospheric WV absorption at 940 nm to correct for the perturbation due to atmospheric WV variability, leading to the development of improved indices, named as ARWI, NARWI-1, and NARWI-3. The performance of these indices was evaluated using the simulated and field spectral reflectance data, as well as Hyperion and GF5 satellite data. Results showed that the new indices were resistant to uncertainty of WV and could be used to deliver improved estimation of canopy water content, with a smaller root-mean-square-error (ARWI: 7.4 mg/cm^2, NARWI-1: 8.3 mg/cm^2, and NARWI-3: 8.8 mg/cm^2) compared to that obtained using the traditional water indices (WI: 8.9 mg/cm^2, NWI-1: 9.4 mg/cm^2, and NWI-3: 16.6 mg/cm^2). The water indices developed in this study, although needing further assessment in wide application scenarios, have great potential for monitoring of vegetation water status using satellite hyperspectral data with reflectance measurement around 970 nm. © *The Authors. Published by SPIE under a Creative Commons Attribution 4.0 Unported License. Distribution or reproduction of this work in whole or in part requires full attribution of the original publication, including its DOI.* [DOI: 10.1117/1.JRS.14.034504]

1 Introduction

Information on canopy vegetation water content is important for assessing vegetation water stress, crop yields, ecosystem functioning, and wildfire risks.[1–4] Remote sensing data provide an opportunity to determine vegetation water status at a large spatial scale. Three variables measuring vegetation water content, including the fuel moisture content (FMC), the equivalent water thickness (EWT), and the canopy water content (CWC), are often estimated from remote sensing data. FMC is defined as the ratio between the water quantity and the dry weight (DW).[5] EWT refers to the amount of water per unit leaf area, while CWC is the total CWC per unit ground area.[6–9] CWC is also named as canopy EWT in some studies.[8,10] Estimation of FMC from remote sensing data is considered more difficult, since leaf dry matter is required for the estimation.[11,12] CWC has been found to be better estimated from remote sensing data, possibly because it is dependent on leaf area index (LAI), which contributes to total reflectance in water absorption bands.[2,13,14]

Vegetation water indices are simple and are commonly used for estimating vegetation water content from hyperspectral or multispectral remote sensing data.[15,16] There are several water absorption features in the near-infrared (NIR, 0.7 to 1.0 μm) and shortwave-infrared (SWIR,

---

*Address all correspondence to Liangyun Liu, E-mail: liuly@radi.ac.cn

1.0 to 2.5 μm) regions. The normalized difference water index (NDWI) using water absorption at 1240 or 1600 nm was developed as an indicator of vegetation water content using Landsat, SPOT, and MODIS data.[17–20] However, absorption by liquid water in vegetation and background soil is too strong in the SWIR region, hence signal returned from canopy is quite weak at these water absorption wavelengths.[21–23] Due to greater penetration of light into the vegetation canopy in the NIR spectral range, the water absorption band at 970 nm has been found to be better for retrieval of canopy water.[5] The reflectance water index (WI, R_{900}/R_{970}) developed in Ref. 21 has been used to estimate plant water content for different vegetation types.[11,22] A normalized water index [NWI-1 = $(R_{970} - R_{900})/(R_{970} + R_{900})$] has been proposed based on reflectance at 970 and 900 nm for wheat water status monitoring.[24] Through changing the reference band at 900 nm in NWI-1, other three normalized water indices have been proposed, e.g., NWI-2 using 850 nm, NWI-3 using 880 nm, and NWI-4 using 920 nm, for vegetation water estimation.[24,25] Among the above indices, NWI-3 was the most effective for canopy water status monitoring.[26] Indices based on the 970-nm absorption feature are supported by some silicon photodiode sensors limited to below 1100 nm.[27–29]

Knowledge of atmospheric aerosol optical thickness (AOT) and water vapor content (WV) is needed in atmospheric correction for retrieving surface reflectance and deriving vegetation indices. However, retrievals of the two variables have considerable uncertainty. Using MODIS AOT and WV products as an example, uncertainty in MODIS AOT product was found to be $\pm(0.05 + 0.15 * \text{AOT})$ over land,[30,31] while uncertainty in MODIS WV product was found to be 10.4%.[32] Uncertainties in aerosol retrievals induces the largest error in surface reflectance retrieval in the visible bands, which impacts the calculation of visible-NIR-based vegetation indices, such as the normalized difference vegetation index (NDVI) and the soil-adjusted vegetation index.[33,34] To reducing this effect, the atmospherically resistant vegetation index (ARVI)[35] and the enhanced vegetation index[36] have been developed to account for impacts of aerosol on NDVI.[37] Similarly, uncertainty in WV will induce uncertainty in NIR reflectance and vegetation water indices, since absorption features of liquid water and WV overlap.[38,39] NDWI using SWIR water absorption band was developed to be less sensitive to atmospheric effect through radiative transfer (RT) simulation.[17]

To our knowledge, uncertainty in 970-nm-based water indices due to atmospheric correction errors has not been evaluated. It is thus important to improve the performance of these water indices under atmospheric perturbation. The objectives of this study, therefore, were: (1) to assess the impact of atmospheric WV content on the 970-nm-based water indices; (2) to develop optimization method for improving these indices under atmospheric perturbation; and (3) to assess the sensitivity of these new indices and their performance of estimating vegetation water status. Since almost all the current water indices are more sensitive to CWC than to FMC and EWT,[2,13,14] only CWC is employed to evaluate the performance of different water indices for estimating vegetation water status. In this paper, canopy and atmospheric RT models are used to simulate canopy reflectance data for developing new atmospherically resistant vegetation water indices, by integrating WV absorption peak around 940 nm (Sec. 2). The results of parameterization of developed new water indices are introduced in Sec. 3.1, and the robustness of the parameterization is assessed and presented in Sec. 3.2. The effects of atmospheric WV on the water indices are assessed using simulated spectral reflectance data in Sec. 3.3. The water indices are then assessed for estimation of CWC using the simulated spectral data (Sec. 3.4) and the field spectral reflectance data (Sec. 3.5). In addition, the sensitivity of satellite-based water indices to WV effect is evaluated using Hyperion and GF5 hyperspectral data in Sec. 3.6. Discussion on the uncertainties and limitations of the atmospherically resistant water-sensitive indices are presented in Sec. 4.

2 Materials and Methods

2.1 Wheat Field Dataset

Field data were collected in a winter wheat experiment in 2002 at the National Precision Agriculture Experimental Base in Xiaotangshan, Changping District, Beijing, China (40°10.6′ N, 116°26.3′E).[40] The study site is located in a warm temperature zone and has a continental
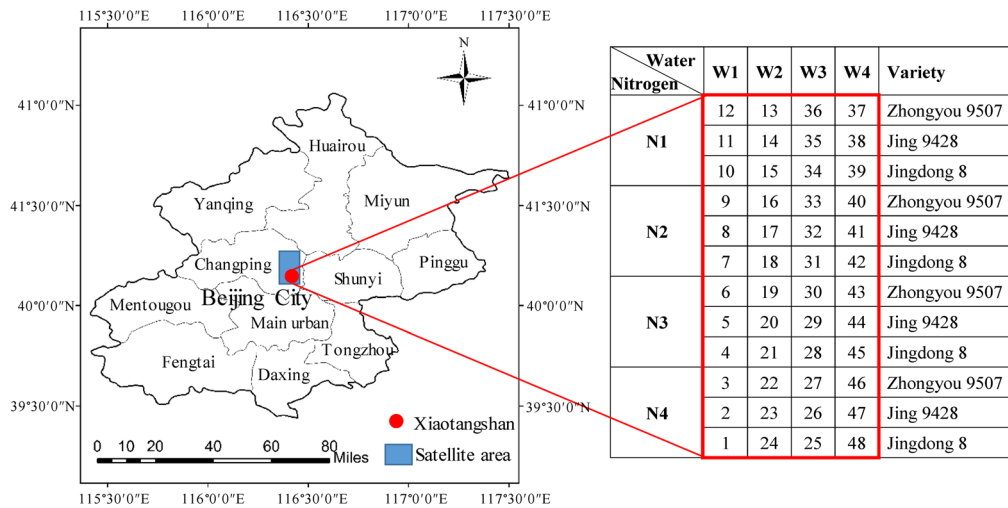
Fig. 1 The study area and winter wheat experiment plots in Xiaotangshan, Beijing, in 2002. The numbers in the red box are the sequence numbers of plots. N1 to N4 represent nitrogen applications of 0, 150, 300, and 450 kg/ha, respectively; W1 to W4 represent water application of 0, 225, 450, and 675 m^3/ha, respectively.

climate. The annual mean temperature is 13.8 deg and average annual precipitation is 507.7 mm. In the field experiment, three winter wheat varieties, Zhongyou 9507, Jing 9428, and Jingdong 8, were seeded in 48 plots with four levels of nitrogen fertilization (N1: 0, N2: 150, N3: 300, and N4: 450 kg/ha) and four water application levels (W1: 0, W2: 225, W3: 450, and W4: 675 m^3/ha). Each plot is 32.4 m × 30 m. The study area and winter wheat experiment design are shown in Fig. 1.

Canopy CWC and spectral reflectance data were collected at the tillering and stem elongation stages, resulting a total of 96 samples. In each sample, a 1-m^2 area of winter wheat was chosen for canopy spectral reflectance measurements as well biophysical and biochemical parameter. Canopy spectral reflectance was measured using a FieldSpec spectrometer (Analytical Spectral Devices, Boulder, Colorado, USA), at the time between 10:00 am and 2:00 pm local time. Leaves were sampled and taken for laboratory analysis to determine the CWC on the same day. The CWC is the weight of foliar water per unit area of ground and is the product of the EWT and the LAI.[10,41] All fresh leaf samples within the sampling area were weighed immediately to obtain fresh weight (FW) and then were oven-dried for 48 h at 60 deg to obtain the DW. Leaf area was manually measured. EWT was calculated as[7]

$$EWT = (FW - DW)/AREA_{Leaf}, \tag{1}$$

where $AREA_{Leaf}$ is the total area of the sampled fresh leaves, calculated as the ratio of DW to specific leaf weight. If EWT and LAI are measured, CWC is then calculated as[41]

$$CWC = EWT \times LAI. \tag{2}$$

2.2 Satellite Hyperspectral Data

Satellite hyperspectral data covering the experiment site were acquired by the Hyperion sensor onboard NASA's EO-1 satellite on April 7, 2003 and May 20, 2004, and by the AHIS sensor onboard China's GF5 satellite on March 18, 2019 and September 1, 2019. The Hyperion sensor collects the upwelling radiance in 242 spectral bands, with 10-nm spectral resolution, 30-m spatial resolution, and 7.5-km swath width. It has a single telescope and consists of two spectrographs, one covering the visible and NIR wavelengths, and the other covering SWIR wavelengths. The GF5 AHSI sensor has 330 spectral channels spanning from 0.4 to 2.5 μm

with 30-m spatial resolution and 60-km swath width. The spectral resolution is about 5 nm in visible-NIR range (0.4 to 1.0 μm) and 10 nm in SWIR range (1.0 to 2.5 μm).[42]

The Hyperion and GF5 data were processed to derive surface reflectance using the Fast Line-of-sight Atmospheric Analysis of Spectral Hypercubes (FLAASH) module[43] in the ENVI software. The FLAASH module uses the MODTRAN RT code for atmospheric correction. AOT was retrieved from the Hyperion data using the FLAASH module. Sensitivity of water indices to atmospheric condition was assessed by changing WV in atmospheric correction.

2.3 *Simulation of Spectral Reflectance Data*

In order to analyze the effect of the atmospheric correction on vegetation water indices, atmospheric correction was conducted using a vegetation RT model and an atmospheric RT model, to generate an error-free canopy reflectance dataset—which assumes that the atmospheric correction is accurate—and an inaccurately retrieved reflectance dataset. Simulation of spectra reflectance data using RT models helps to obtain enough samples with a wide range of conditions that actual field experiments cannot achieve.

First, the PROSAIL model, as a combination of the PROSPECT leaf model[44] and the SAIL canopy reflectance model,[45] was used to simulate the error-free canopy reflectance for a range of leaf and canopy parameter values. The PROSAIL model is optimized for a spatially continuous canopy, applicable for a closed winter wheat canopy. CWC can be calculated from EWT and LAI using Eq. (2). Both EWT and LAI are input parameters to the PROSAIL model. EWT ranged from 4 to 24 mg/cm^2 and LAI ranged from 1 to 6 in PROSAIL model simulation. A range of leaf dry matter (C_m) and leaf structure parameter (N) were considered in simulation experiment. The influence of leaf chlorophyll content on reflectance in the 970-nm range is negligible.[41] Thus, leaf chlorophyll parameter can be fixed to a nominal value. The average leaf inclination angle (ALA) was set to 35 deg for winter wheat. A typical spectra of bright soil was used for Xiaotangshan site. The Sun-sensor geometry parameters are corresponding to the location and time of the above winter wheat field experiment. A list of the parameters used in the PROSAIL model simulation is presented in Table 1.

The 6S model[46] was then used to simulate atmospheric effect on retrieving of reflectance and vegetation water indices. Using the forward mode of the 6S model with true values for atmospheric parameters, canopy reflectance data simulated by the PROSAIL model were converted into top-of-atmosphere spectral data. For a sunny day, a true value of AOT at 550 nm (AOT$_{550}$) was set to 0.2 and a true value of WV was set to 2.0 g/cm^2. An altitude of 40 m of Xiaotangshan site was used. Other atmospheric parameters in the 6S model were set to their default values in this simulation.

Table 1 Parameters used in the PROSAIL model for simulation of canopy spectral reflectance.

Parameter	Value range	Unit
LAI	1 to 6, in steps of 1	—
Leaf EWT	4 to 24, in steps of 4	mg/cm^2
Leaf dry matter content (C_m)	0.004, 0.006	g/cm^2
Leaf structure parameter (N)	1.6, 1.8	—
Leaf chlorophyll-a and -b content (C_{ab})	50	μg/cm^2
ALA	35	deg
Soil background	Bright soil	—
Sun zenith and azimuth (θ_s, φ_s)	(30, 0)	deg
View zenith and azimuth angle (θ_v, φ_v)	(0, 0)	deg
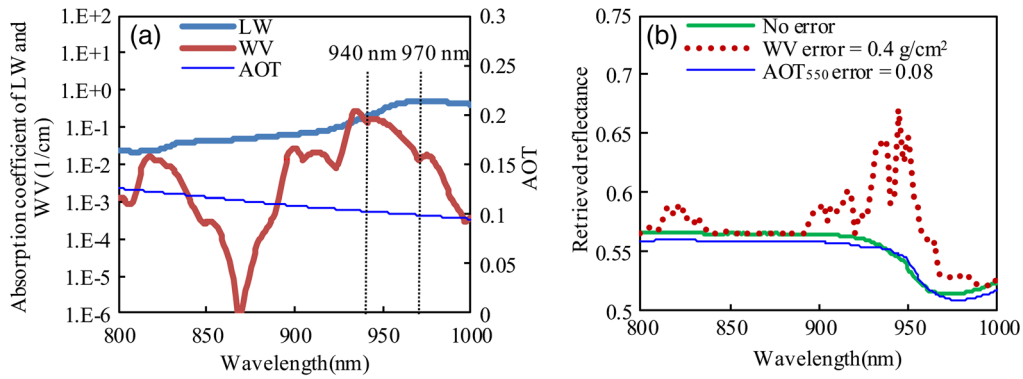
Fig. 2 (a) A typical AOT spectrum for AOT at 550 nm (AOT$_{550}$) set to 0.2 and absorption spectra of leaf liquid water (LW) and WV between 800 and 1000 nm; (b) surface reflectance with and without atmospheric correction errors, obtained from the simulation experiment. The error of AOT$_{550}$ is 0.08, and the error of WV is 0.4 g/cm^2.

Third, inaccurate reflectance data were simulated from the top-of-atmosphere data simulated above using the 6S model in its reverse mode. As can be seen from Fig. 2(a), the reflectance changes due to AOT are relatively spectrally smooth and flat compared to those due to the selective absorption by atmospheric WV.[47] In addition, the effect of aerosols on the shortwave infrared bands is much smaller than that in the visible bands.[17,46] Thus, atmospheric correction at around 970 nm is more sensitive to errors in WV than to errors in AOT, and the impact of AOT is negligible to reflectance retrieval,[30,32] which are also shown in Fig. 2. However, when a 20% relative error was added to WV at 2.0 g/cm^2 (i.e., 0.4 g/cm^2), large errors in the simulated reflectance can be introduced, especially at the NIR WV absorption band [Fig. 2(b)]. We intended to reduce atmospheric WV effect on spectral water indices based on 970-nm absorption. Referring to the accuracy level of MODIS WV production,[32] errors in the WV were set to ±0.1, ±0.2, ±0.3, and ±0.4 g/cm^2 for the simulation experiment in the atmospheric correction step.

2.4 Vegetation Water Indices

Different water indices may be impacted differently by the errors in WV for atmospheric correction. In this study, three 970-nm-based water indices, WI, NWI-1, and NWI-3, were selected for testing their sensitivity to atmospheric WV effect. These indices use reflectance at 970 nm and reflectance at a reference wavelength nearby: 900 nm for WI and NWI-1, 880 nm for NWI-3. Compared to 970 nm, absorption by liquid water in vegetation canopy in these reference wavelengths is weaker.[21,24,25] WI is calculated as the ratio of the reflectance at the 900-nm reference wavelength to that at the water absorption peak of 970 nm:[21]

$$\text{WI} = R_{900}/R_{970}, \tag{3}$$

where R_{900} and R_{970} are the surface reflectance at 900 and at 970 nm, respectively. NWI-1 is formulated as[24]

$$\text{NWI-1} = (R_{970} - R_{900})/(R_{970} + R_{900}), \tag{4}$$

and NWI-3 is formulated as[25]

$$\text{NWI-3} = (R_{970} - R_{880})/(R_{970} + R_{880}). \tag{5}$$

In addition, NDWI using reflectance at 1240 nm (NDWI$_{1240}$) and NDWI at 1640 nm (NDWI$_{1640}$) were also selected for comparison with 970-nm-based water indices, since the two NDWIs have been considered to be less sensitive to atmospheric effect.[17–19] NDWI$_{1240}$ and NDWI$_{1640}$ are calculated as

$$\text{NDWI}_{1240} = (R_{860} - R_{1240})/(R_{860} + R_{1240}), \tag{6}$$

and

$$\text{NDWI}_{1640} = (R_{860} - R_{1640})/(R_{860} + R_{1640}). \qquad (7)$$

2.5 *Approach to Compensating Atmospheric Water Vapor Effects*

To reduce the effect of atmospheric WV on 970-nm-based water indices, the self-correction approach of ARVI[35] was adopted in this study by introducing WV absorption band at 940 nm. ARVI uses a combination of NDVI and the blue band reflectance to correct the atmospheric effects, and the resistance of ARVI to atmospheric aerosol effect is accomplished using the difference in sensitivity of the blue and red channels to aerosols. Even though the absorptions of atmospheric WV and plant liquid water may overlap, their absorption peaks in 800 to 1000 nm range are different by about 30 nm [Fig. 2(a)]. When there is error in WV used for atmospheric correction, the changes in the retrieved surface reflectance at the 940-nm wavelength will be larger than that in nearby wavelengths. Therefore, it is possible to separate the contributions from canopy water absorption and reference wavelength for water index calculation by incorporating reflectance at 940 nm.

First, to design new spectral water indices resistant to atmospheric WV effect, we adjusted the reflectance at 970 nm and the reference wavelength using the reflectance at 940 nm (referred to as R'_λ). The WV absorption peak at 940 nm is impacted more by WV, which can be exploited to correct reflectance in other bands less affected by errors in atmospheric conditions. We assume that R'_λ obtained this way is resistant to atmospheric effects:

$$R'_\lambda = R_\lambda - k_\lambda \times R_{940} = R_{\lambda,\text{ture}} - k_\lambda \times R_{940,\text{ture}}, \qquad (8)$$

where λ is a given wavelength in the range 800 to 1000 nm, and k_λ is the correction coefficient that makes R'_λ resistant to WV effect; R_λ is the surface reflectance retrieved through atmospheric correction, which may bring errors caused by inaccurate knowledge of atmospheric WV. As a special case of R_λ, $R_{\lambda,\text{true}}$ is the result using the accurate WV thus represents the true surface reflectance. In contrast to $R_{\lambda,\text{true}}$, the values of R'_λ includes errors caused by the atmospheric WV effect.

Second, it is a key step to derive the correction coefficient k_λ in Eq. (8). We transformed Eq. (8) into Eq. (9)

$$R_\lambda - R_{\lambda,\text{ture}} = k_\lambda \times (R_{940} - R_{940,\text{ture}}). \qquad (9)$$

Equation (9) means that change of reflectance from its true value due to inaccurate WV correction at any wavelength λ is proportional to that at 940 nm:

$$\Delta(R_\lambda) = k_\lambda \times \Delta(R_{940}). \qquad (10)$$

If the above assumption is valid, k_λ can be obtained through regression analysis, using simulated retrieved reflectance dataset with variable values of WV input shown in Table 2.

Following the above steps, we developed a new simple ratio index based on WI through integration of the band at 940 nm, named as an atmospherically resistant water index (ARWI), which is the ratio of R'_{900} to R'_{970}. This ARWI index can be calculated using the surface reflectances retrieved using atmospheric correction at 900, 940, and 970 nm, expressed as

$$\text{ARWI} = \frac{R'_{900}}{R'_{970}} = \frac{R_{900} - k_{900} \times R_{940}}{R_{970} - k_{970} \times R_{940}}. \qquad (11)$$

A new normalized, atmospherically resistant water index based on NWI-1 (NARWI-1) using the band at 940 nm also is designated as

$$\text{NARWI-1} = \frac{R'_{970} - R'_{900}}{R'_{970} + R'_{900}} = \frac{R_{970} - R_{900} - (k_{970} - k_{900}) \times R_{940}}{R_{970} + R_{900} - (k_{970} + k_{900}) \times R_{940}}. \qquad (12)$$

Table 2 Parameters used in the 6S model for atmospheric correction simulation.

Parameter	Value range	Unit
WV content	1.6 to 2.4, in steps of 0.1	g/cm^2
AOT at 550 nm (AOT$_{550}$)	0.2, 0.28, 0.44	—
Aerosol type	Land, ocean, city	—
Ozone content	0.3	atm-cm
Sensor height	700	Km
Altitude	40	M
Sun zenith and azimuth (θ_s, φ_s)	(30, 0)	deg
View zenith and azimuth angle (θ_v, φ_v)	(0, 0)	deg

Another new normalized, atmospherically resistant water index based on NWI-3 (NARWI-3) using the reference wavelength of 880 nm is calculated as

$$\text{NARWI-3} = \frac{R'_{970} - R'_{880}}{R'_{970} + R'_{880}} = \frac{R_{970} - R_{880} - (k_{970} - k_{880}) \times R_{940}}{R_{970} + R_{880} - (k_{970} + k_{880}) \times R_{940}}. \tag{13}$$

3 Results and Analysis

3.1 Determination of Correction Coefficients

Using simulated data, the relationship between reflectance changes at 970 and 940 nm due to atmospheric WV perturbation is shown in Fig. 3. In the simulation, WV was changed in a range 0.4 g/cm^2 above and below the true WV at 2.0 g/cm^2. It can be observed that the reflectance changes at 970 nm from the true values were strongly correlated with that at 940 nm ($R^2 = 0.998$). The correction coefficient in Eqs. (8)–(10) for 970 nm (k_{970}) was 0.394.

Using the same approach, the correction coefficients k_λ in Eqs. (8)–(10) for any wavelength between 860 nm and 1000 nm can also be determined, and the results are shown in Fig. 4. The correction coefficient at different wavelengths varies between 0 and 2.8. As shown by the coefficient of determination, the linear relationships are strong between reflectance changes at 940 nm and at most of wavelengths below 860 nm. The coefficient was 0.534 for 900 nm (k_{900}), whereas 0 for 880 nm (k_{880}), which means that reflectance at 880 nm is hardly affected by variation in WV. The results for the three wavelengths are reported in Table 3, and the values of k_{970}, k_{900}, and k_{880} can be used to derive the improved water indices given in Eqs. (11)–(13).
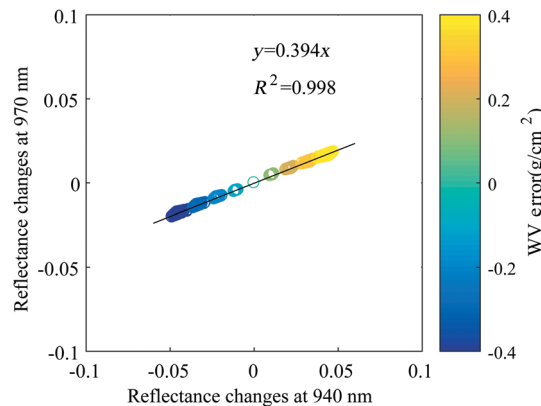
Fig. 3 The relationship between reflectance changes induced by the WV effect at 940 nm and that at 970 nm, illustrated by the WV content error.
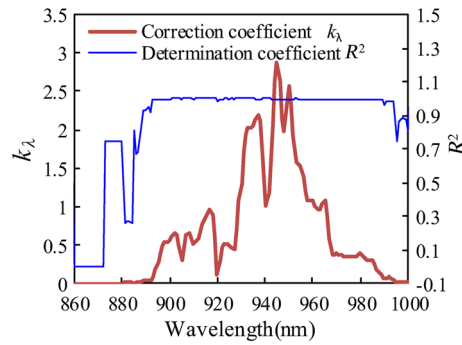
Fig. 4 The correction coefficients (k_λ) against WV effect at different wavelengths and the corresponding significant coefficient of determination (R^2) calculated based on the simulations using the PROSAIL model and the 6S model. In simulation, WV content is set to 2.0 ± 0.4 g/cm^2.

Table 3 The correction coefficients for new 970-nm-based atmospherically resistant water indices using WV absorption wavelength at 940 nm.

Correction coefficient	Value	R^2
k_{970}	0.394	0.998
k_{900}	0.534	0.998
k_{880}	0.000	—

3.2 Influences of Atmospheric Correction Inputs in Parameterization of New Water Indices

3.2.1 Influence of true water vapor content

Compared with the fixed WV true value of 2.0 g/cm^2 for simulation in Sec. 3.1, we changed true values for the WV (1.6, 2.0, 2.4 g/cm^2). Figure 5 shows the calculation results of k_{970} with variations in settings of true value of WV.

Variation in WV true value only makes small changes of the correction coefficients ($k_{970} = 0.390$) in Fig. 5, compared to that result ($k_{970} = 0.394$) for the fixed WV true value of 2.0 g/cm^2 in Fig. 4 and Table 3. Thus, it implies that variations in settings of true value of WV true in simulation have little influence on parameterization of the new water spectral indices in Eqs. (11)–(13).
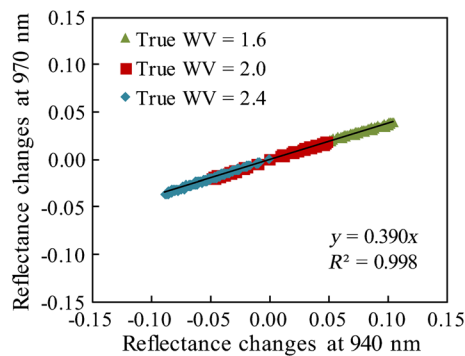
Fig. 5 The relationship between the reflectance changes induced by atmospheric WV content at 940 nm and the changes at 970 nm, as characterized by the true value of WV. The true values of WV are set to 1.6, 2.0, and 2.4 g/cm^2, respectively.
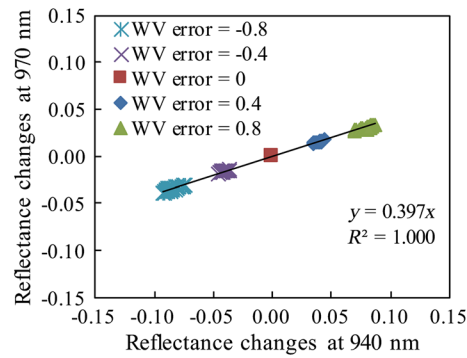
Fig. 6 The relationship between the reflectance changes induced by atmospheric WV content at 940 nm and the changes at 970 nm, as characterized by the WV error ranging from −0.8 to 0.8 g/cm^2.

3.2.2 Influence of water vapor errors

The influence of WV in the parameterization of the new water indices was tested, and the results were shown in Fig. 6. The strong linear relationship indicates that the correction efficient is stable for different levels of WV error (ranging from −0.8 to 0.8 g/cm^2).

3.2.3 Influence of aerosol errors

The influence of aerosol in the parameterization of the new water indices was also tested, and the results were shown in Fig. 7. Aerosol will influence the assumed relationship in Eqs. (9) and (10) but is acceptable if the AOT_{550} error is retained below 0.1.

3.3 Water Vapor Effect Assessment on Calculation of Water Indices Using Simulated Spectra

The root mean square error (RMSE) is regularly employed in accuracy evaluation. Relative root mean squared error (RRMSE) can be considered as a normalized RMSE metrics. Because different water indices own different value ranges, RRMSE is a better matrix to increase the comparability of the sensitivity of calculation of different water indices to the WV effect. The values of water indices with atmospheric WV errors were compared to those corresponding error-free values, and R^2 and RRMSE were calculated in Table 4.
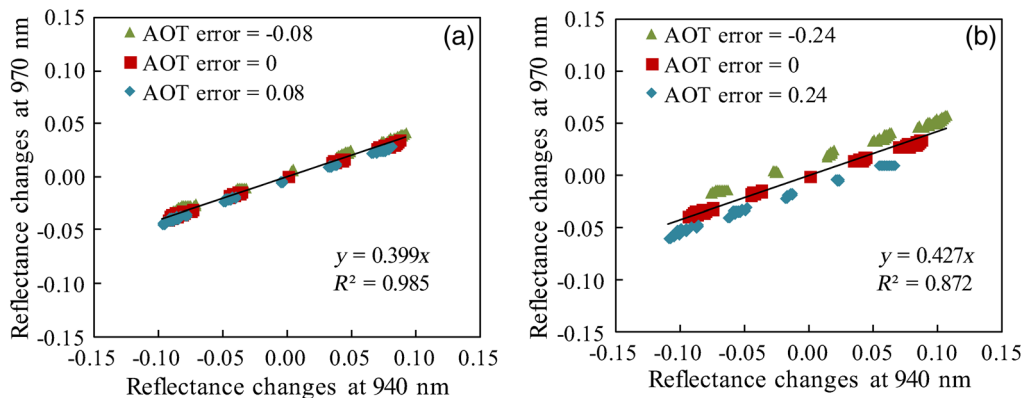
Fig. 7 The relationship between the reflectance changes induced by both WV and aerosol effect at 940 nm and the changes at 970 nm, with different AOT at 550 nm (AOT_{550}) error of (a) ±0.08 and (b) ±0.24.

Table 4 Errors between vegetation water indices with atmospheric correction errors and the corresponding error-free water indices. ARWI is improved from WI, NARWI-1 is improved from NWI-1, and NARWI-3 is improved from NWI-3.

Vegetation water index	R^2	RRMSE (%)
WI	0.985	12.0
ARWI	1.000	2.7
NWI-1	0.985	12.0
NARWI-1	0.999	2.6
NWI-3	0.856	41.0
NARWI-3	0.999	2.8
$NDWI_{1240}$	0.999	0.7
$NDWI_{1640}$	1.000	0.2

Table 4 shows that there is little difference between $NDWI_{1240}$ with atmospheric correction errors and the error-free $NDWI_{1240}$, and a similar situation occurred with $NDWI_{1640}$. That implies that NDWIs using SWIR water absorption band are hardly affected by WV input error in atmospheric correction. However, all three existing 970-nm water indices (WI, NWI-1, and NWI-3) are more sensitive to WV errors in atmospheric correction process than NDWIs.

Table 4 also shows that all three improved water indices including ARWI, NARWI-1, and NARWI-3 can minimize their WV effect as NDWIs. The linear regression between the values between ARWI, NARWI-1, and NARWI-3 with atmospheric correction errors and their error-free values shows a high correlation (R^2 more than 0.99), with the better RRMSE (less than 3%) than the RRMSE results (more than 10%) of WI, NWI-1, and NWI-3.

NWI-3 is most affected by the WV effect. The R^2 of regression between NWI-3 values with atmospheric correction error and error-free NWI-3 values is only 0.856 with the largest RRMSE of 41.0%. Compared with NWI-3, the RRMSE calculated between NARWI-3 with atmospheric correction errors and its error-free values was improved to 2.8%. The scatter plot between NWI-3 with atmospheric correction errors and its error-free values appears more discrete than its improved index NARWI-3, as shown in Fig. 8. It means that the improvement of NARWI-3 from NWI-3 against atmospheric WV effect is rather obvious.
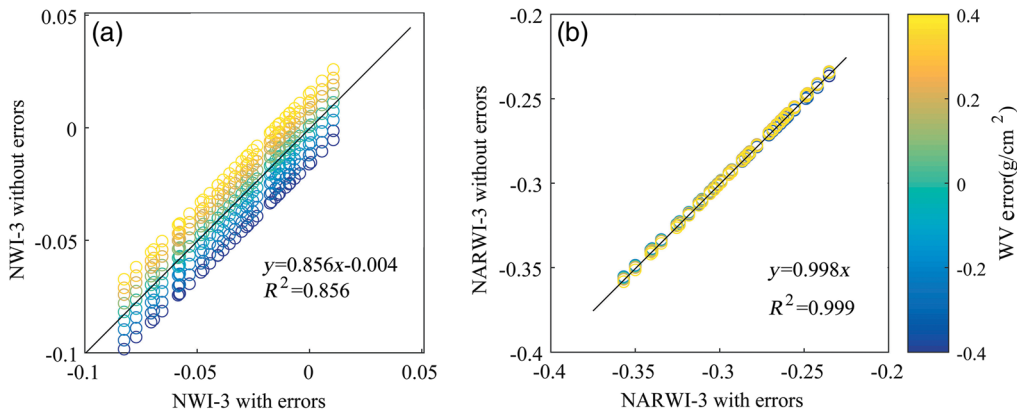
Fig. 8 Scatter plots of (a) NWI-3 and (b) NARWI-3 with atmospheric correction errors caused by inaccurate WV content inputs against error-free values of the two water indices, as characterized by the WV input error.

3.4 *Performance of Water Indices for Vegetation Water Content Estimation Using Simulated Spectra*

Based on simulated datasets without atmospheric correction errors, regression models were built to assess relationships between CWC and water indices. The results in Fig. 9 show all of these eight water indices had high correlations with CWC (R^2 more than 0.94), when the atmospheric correction is error-free.

Based on simulated dataset with atmospheric correction errors, scatter plots of the CWC and the selected eight water spectral indices were built (Fig. 10). The three existing water indices with atmospheric correction errors have lower correlations with the CWC (WI: $R^2 = 0.937$, NWI-1: $R^2 = 0.929$, NWI-3: $R^2 = 0.807$) than those result of their improved water indices (ARWI: $R^2 = 0.958$, NARWI-1: $R^2 = 0.946$, NARWI-3: $R^2 = 0.942$). In addition, all of the three improved water indices with atmospheric correction errors have similarly good correlations with the CWC (Fig. 10), compared with their result without atmospheric correction errors (Fig. 9). Like the three improved 970-nm-based water indices, the two NDWIs also keep high correlations with CWC, whether there is atmospheric correction error or not.

Using models presented in Fig. 9, CWC was estimated from the simulated datasets with and without atmospheric correction errors (Table 5). When there are no atmospheric WV errors in simulated dataset, both the existing and developed 970-nm-based water indices produced similar results of CWC estimation with R^2 from 0.942 to 0.958 and RMSE from 7.3 to 8.6 mg/cm^2. The two NDWIs also obtained good R^2 in CWC estimation, and only NDWI$_{1640}$ produced a large CWC RMSE more than 10 mg/cm^2.

As shown in Table 5, the three developed atmospherically resistant water indices improve estimation of the CWC, compared with their three original water indices against to the WV effect. Compared with their results based on simulated dataset without atmospheric correction
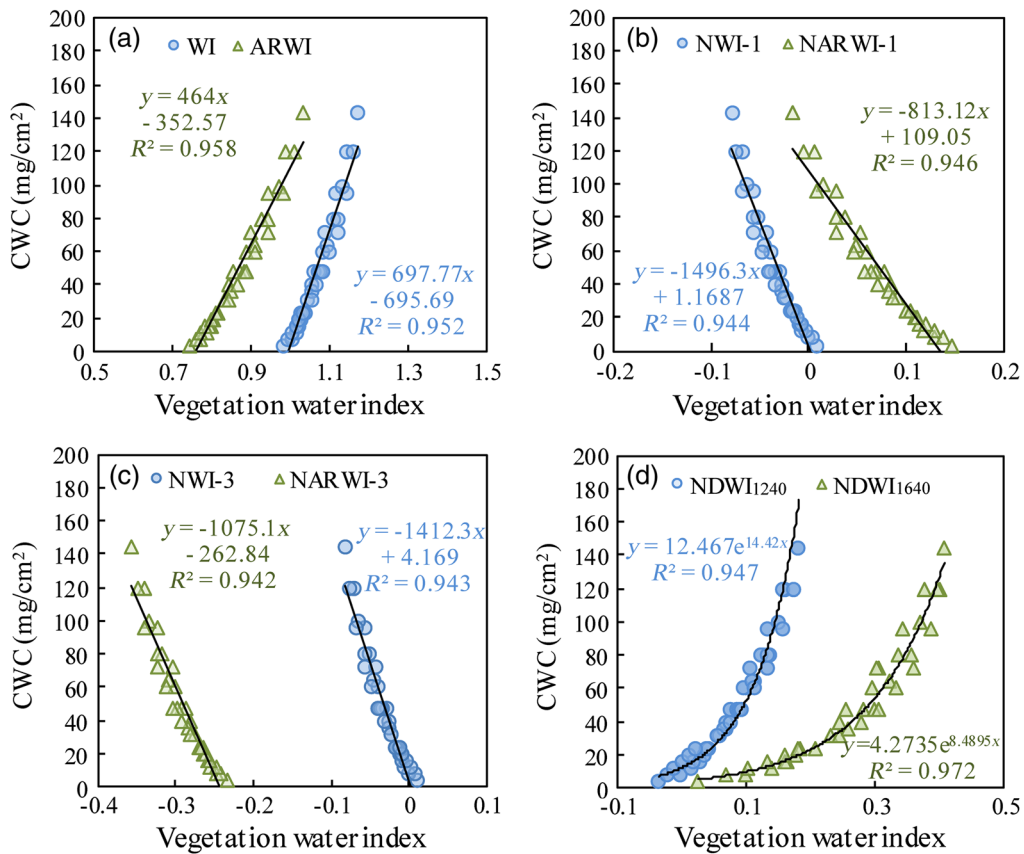
Fig. 9 Relationship between CWC and vegetation water indices (a) WI and ARWI, (b) NWI-1 and NARWI-1, (c) NWI-3 and NARWI-3, and (d) NDWI based on a simulated dataset without atmospheric correction errors.
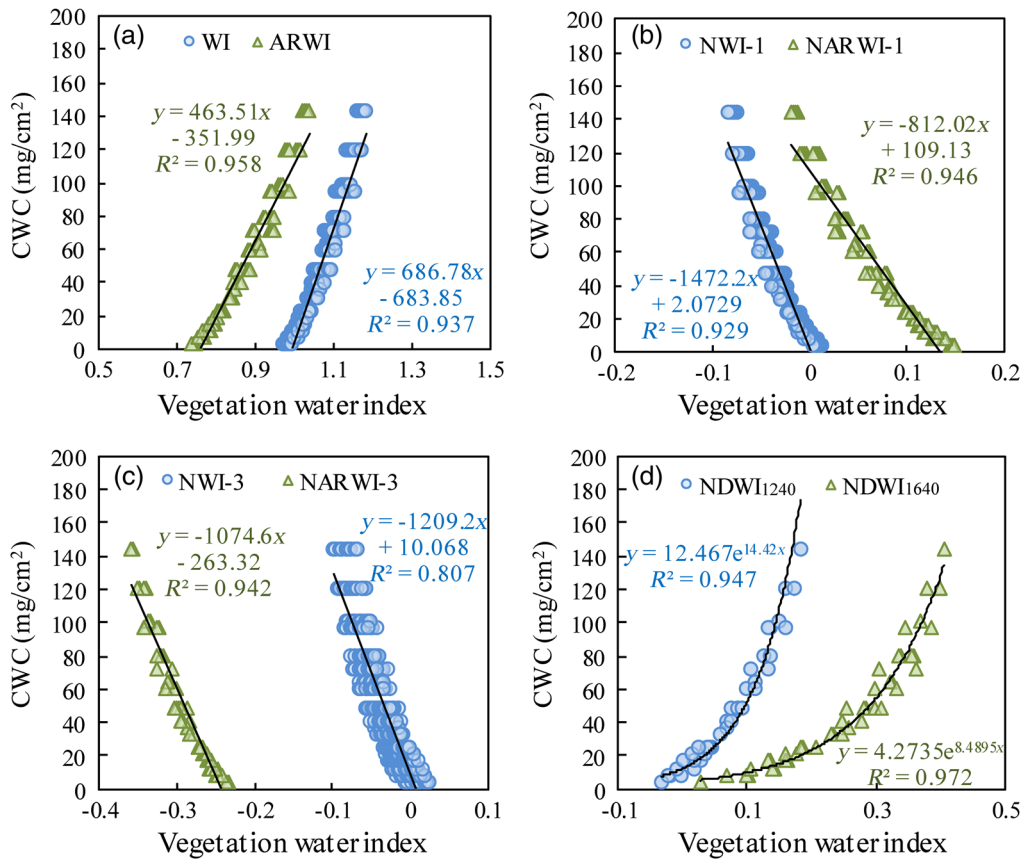
Fig. 10 Relationship between CWC and vegetation water indices (a) WI and ARWI, (b) NWI-1 and NARWI-1, (c) NWI-3 and NARWI-3, and (d) NDWI based on simulated dataset with atmospheric correction errors.

Table 5 Accuracy assessment for the estimation of CWC by vegetation water indices based on simulated datasets with and without WV content errors. The used water index-CWC regression relations from error-free data simulated using PROSAIL model (as shown in Fig. 9) were shown (y denotes CWC and x denotes water index).

Vegetation water index	Water index-CWC relation	Simulated dataset without WV errors		Simulated dataset with WV errors	
		R^2	RMSE (mg/cm^2)	R^2	RMSE (mg/cm^2)
WI	$y = 697.77x - 695.69$	0.952	7.9	0.938	8.9
ARWI	$y = 464x - 352.57$	0.958	7.3	0.958	7.4
NWI-1	$y = -1496.3x + 1.1687$	0.944	8.5	0.931	9.4
NARWI-1	$y = -813.12x + 109.05$	0.946	8.3	0.946	8.3
NWI-3	$y = -1412.3x + 4.169$	0.943	8.6	0.807	16.6
NARWI-3	$y = -1075.1x - 262.84$	0.942	8.6	0.942	8.8
NDWI$_{1240}$	$y = 12.467e14.42x$	0.958	10.1	0.958	10.0
NDWI$_{1640}$	$y = 4.2735e8.4895x$	0.953	7.8	0.953	7.8
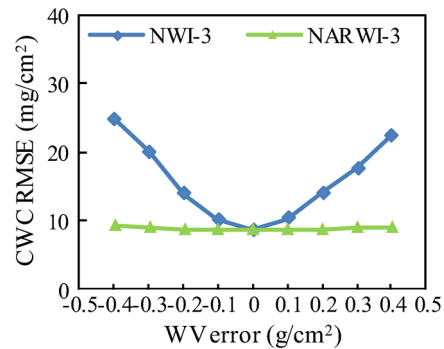
Fig. 11 The RMSE of CWC estimated by NWI-3 and NARWI-3 plotted against the error in the value of the atmospheric WV content in atmospheric correction.

errors, WI, NWI-1, and NWI-3 have much poorer performance of CWC estimation based on simulated dataset with atmospheric correction errors. However, all of three new water indices (ARWI, NARWI-1, and NARWI-3) obtain better estimation of the CWC than their original water indices, for both the simulated dataset with and without atmospheric correction errors. When there are atmospheric correction errors, RMSE of CWC estimation by ARWI is 7.4 mg/cm^2 less than WI (RMSE = 8.9 mg/cm^2), and the CWC estimation result of NARWI-1 (RMSE = 8.3 mg/cm^2) is better than NWI-1 (RMSE = 9.4 mg/cm^2). NARWI-3 has the most improvements of CWC estimation (RMSE: 8.8 mg/cm^2) compared with NWI-3 (RMSE: 16.6 mg/cm^2).

The trend between WV error and the RMSE of CWC estimated using NWI-3 versus NARWI-3 is shown in Fig. 11. The RMSE in the CWC estimated using NWI-3 increases greatly with the increasing error in the atmospheric WV and the maximum RMSE value reach about 25 mg/cm^2, while the RMSE values in the CWC estimated by NARWI-3 remain <10 mg/cm^2. Compared to the estimation of the CWC made using NWI-3, the CWC values estimated by NARWI-3 were more resistant to the WV input errors in atmospheric correction. It can be implied that the greater the error of WV in atmospheric correction, the greater the influence on the CWC estimation by existing 970-nm-based water index; while the result of CWC estimation using new 970-nm-based water index could be resistant to the WV effect.

3.5 Validation of Vegetation Water Content Estimation Using Field Dataset

The previously recalibrated formulae for estimating the CWC derived from the error-free simulated dataset (Fig. 9) were validated with the field data obtained in the Beijing study area. Field reflectance data are regarded as having no atmospheric correction errors. Figure 12 shows the results of CWC accuracy assessment from the observations of winter wheat. All six 970-nm-based water indices can get good CWC estimation with RMSE less than 8 mg/cm^2 and R^2 higher than 0.8. The results of simulated dataset without WV errors (Table 5) and field dataset (Fig. 12) show that both the existing and developed 970-nm-based water indices produced good estimation of the CWC when these error-free reflectance data were used.

Figure 12 also shows that all of six 970-nm-based water indices got a little better estimation of CWC based on the field measured reflectance data than the two NDWIs. The NDWI$_{1640}$−CWC formula produced the CWC estimation with a maximum RMSE, and NDWI$_{1240}$ followed with a second largest RMSE. The validation results of CWC estimation using the two NDWIs also yielded lower R^2 than that using either existing or developed 970-nm-based water indices.

3.6 Sensitivity of Water Index on Atmospheric Correction Errors Using Satellite Data

The impact of atmospheric WV on the selected existing and new water indices was assessed using different satellite hyperspectral data, including the Hyperion and GF5. For calculation
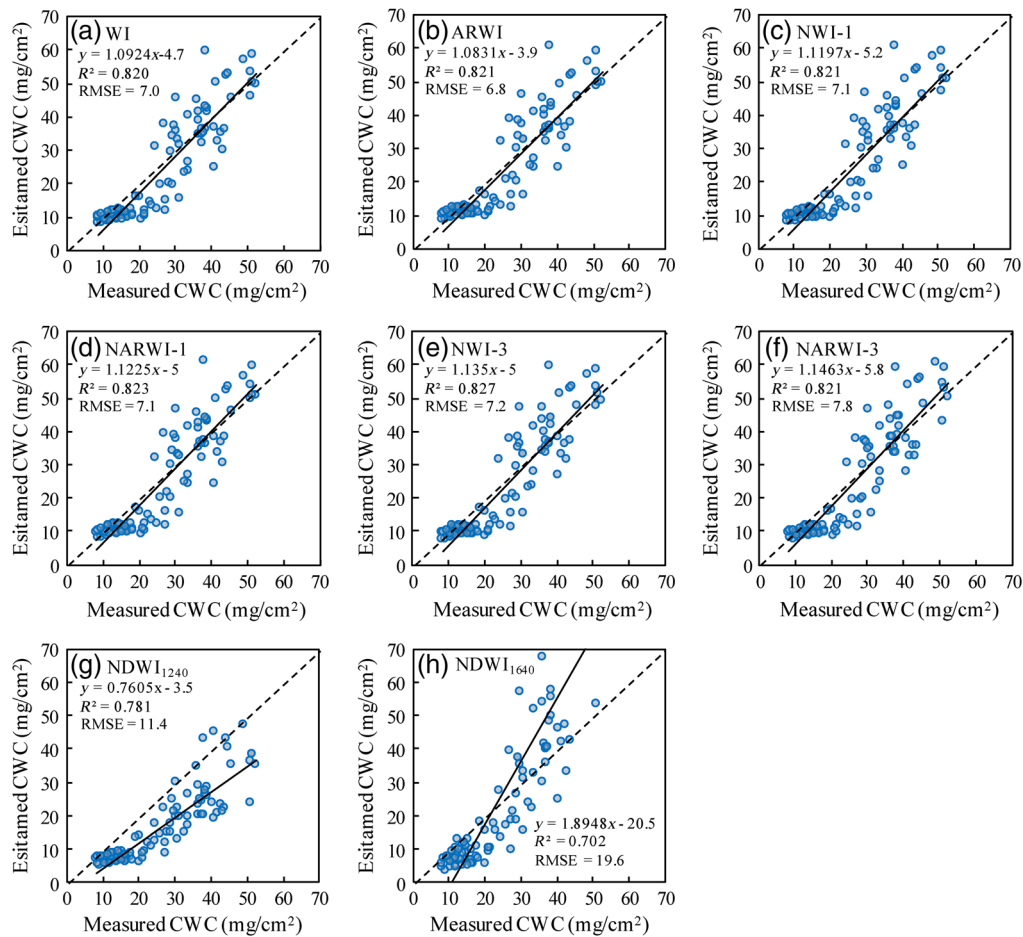
Fig. 12 Scatter plots of CWC predicted by (a) WI, (b) ARWI, (c) NWI-1, (d) NARWI-1, (e) NWI-3, (f) NARWI-3, (g) NDWI$_{1240}$, and (h) NDWI$_{1640}$ against the *in situ* CWC measurements. The field measured reflectance data are regarded as error-free in atmospheric effects.

of the water indices from Hyperion imagery, the wavelength of the channel correspondent to WV absorption peak is 943 nm, and that of vegetation water absorption is 973 nm. The reference channel at 895 nm is chosen for WI, ARWI, NWI-1, and NARWI-1, and 885 nm for NWI-3 and NARWI-3. Figure 4 shows the correction coefficient k_λ at different wavelengths. k_λ for a specific satellite hyperspectral sensor (e.g., Hyperion) could be determined through spectral sampling using the spectral response function, for example 0.187 at 973 nm band, 0.145 for 895 nm band, and 0 for 883 nm band. Using these correction coefficients, the three new atmospherically resistant water indices for Hyperion data are given in Table 6. For GF5 data, the WV absorption peak is at the 942-nm channel, and vegetation water absorption peak is at the 973-nm channel. The reference channels at 899- and 886-nm channels were selected for the water indices. The coefficients for the GF5 are determined as 0.208 for k_{972}, 0.313 for k_{899}. The results are also given in Table 6.

Reflectance was retrieved from the Hyperion and the GF5 hyperspectral data using the FLAASH atmospheric correction module, with the WV parameters set to a range of 0.5 to 2.5 g/cm^2. All the selected 970-nm-based water indices were calculated from the Hyperion and GF5 reflectance data retrieved with WV varying within the given ranges following a normal distribution. Figure 13 shows the calculation results of standard deviation (SD) of the water indices induced by inaccurate atmospheric WV inputs in the FLAASH atmospheric correction module for three land cover types (shown in Fig. 14) of crop (green), grass (blue), and sparse forest (yellow) in the Hyperion and GF5 images. As shown in Fig. 13, the existing 970-nm-based water indices (WI, NWI-1, and NWI-3) are more affected by atmospheric WV effect than the

Table 6 Parameterization expressions of 970-nm-based atmospherically resistant water indices for Hyperion and GF5 satellite hyperspectral data.

Satellite data	New water index	Formula	Correction coefficient	WV channel
Hyperion	ARWI$_{Hyperion}$	$\dfrac{(R_{895} - k_{895} \times R_{943})}{(R_{973} - k_{973} \times R_{943})}$	$k_{973} = 0.187$	943 nm for Hyperion
	NARWI-1$_{Hyperion}$	$\dfrac{[R_{973} - R_{895} - (k_{973} - k_{895}) \times R_{943}]}{[R_{973} + R_{895} - (k_{973} + k_{895}) \times R_{943}]}$	$k_{895} = 0.145$	
	NARWI-3$_{Hyperion}$	$\dfrac{[R_{973} - R_{883} - (k_{973} - k_{883}) \times R_{943}]}{[R_{973} + R_{883} - (k_{973} + k_{883}) \times R_{943}]}$	$k_{883} = 0.000$	
Gf5	ARWI$_{GF5}$	$\dfrac{(R_{899} - k_{899} \times R_{942})}{(R_{972} - k_{972} \times R_{942})}$	$k_{972} = 0.208$	942 nm for Gf5
	NARWI-1$_{GF5}$	$\dfrac{[R_{972} - R_{899} - (k_{972} - k_{899}) \times R_{942}]}{[R_{972} + R_{899} - (k_{972} + k_{899}) \times R_{942}]}$	$k_{899} = 0.313$	
	NARWI-3$_{GF5}$	$\dfrac{[R_{972} - R_{886} - (k_{972} - k_{886}) \times R_{942}]}{[R_{972} + R_{886} - (k_{972} + k_{886}) \times R_{942}]}$	$k_{886} = 0.000$	
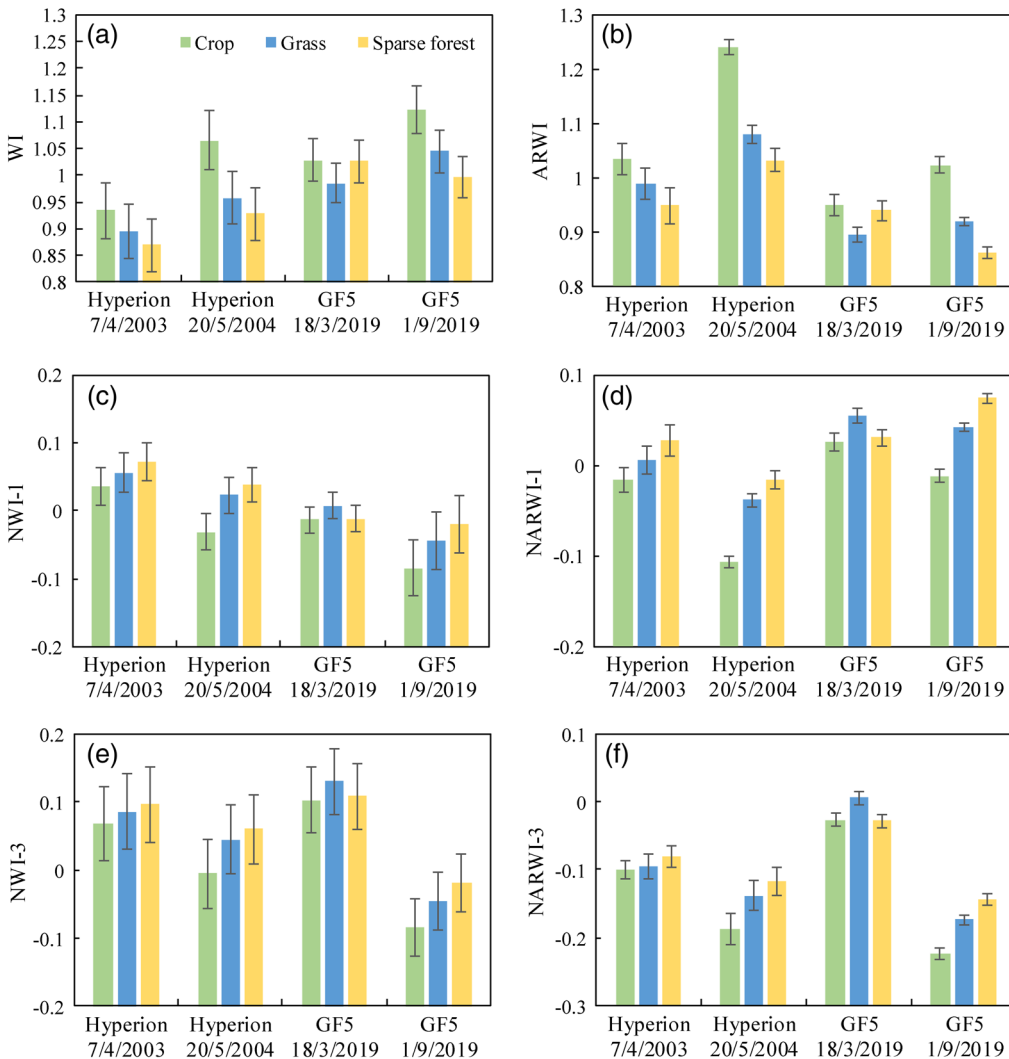
Fig. 13 Calculation result of 970-nm based water indices (a) WI, (b) ARWI, (c) NWI-1, (d) NARWI-1, (e) NWI-3, and (f) NARWI-3 from Hyperion and GF5 retrieved reflectance data against the inaccurate atmospheric water vapor content (WV) inputs in FLAASH module.
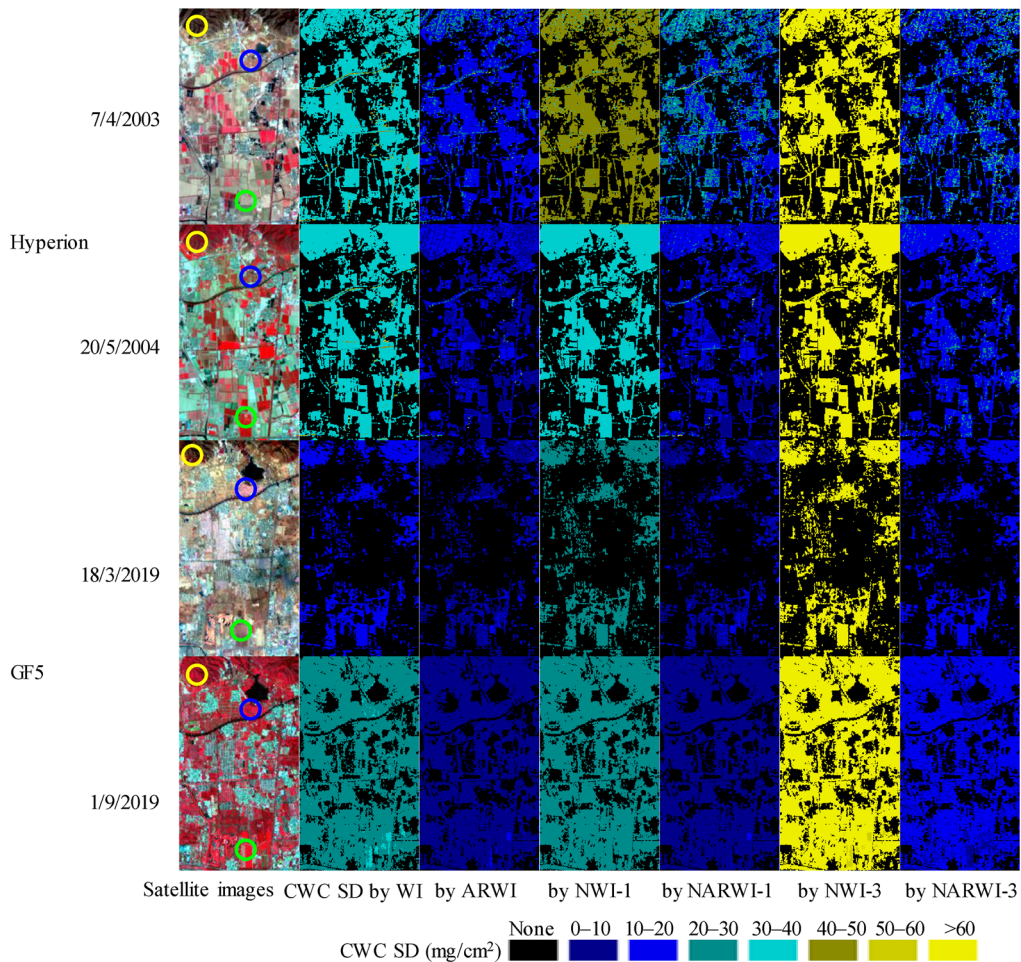
Fig. 14 The SD of CWC derived using 970-nm-based water indices from Hyperion and GF5 data with inaccurate atmospheric WV correction. The green, blue, and yellow circles in the four satellite images on the left represent crop, grass, and sparse forest areas, respectively.

respective improved indices (ARWI, NARWI-1, and NARWI-3), as indicated by the much smaller SD of the improved indices derived for both Hyperion and GF5 satellite data.

Using the developed CWC estimation equations built from error-free simulated data presented in Fig. 9, the SD of CWC derived using different indices from the two Hyperion images and the two GF5 images are calculated (Fig. 14). The results showed that different water indices have different CWC SD. For Hyperion data, most of CWC SD values range between 30 and 50 mg/cm^2 for WI and NWI-1 and are more than 60 mg/cm^2 using NWI-3. When using ARWI, NARWI-1, and NARWI-3, most of CWC SD values are between 0 and 20 mg/cm^2. Similar results can be observed for GF5 (Fig. 14).

The results of both Hyperion and GF5 showed that our three improved 970-nm-based water indices could bring lower uncertainty in CWC estimation against WV effect in atmospheric correction.

4 Discussion

4.1 *Building Robust Vegetation Water Indices Resistant to Atmospheric Effect Using 970-nm Water Absorption Feature*

The focus of this study is on reducing the atmospheric effect on calculation of 970-nm-based water indices. The 940-nm WV absorption feature and the 970-nm vegetation water absorption

feature overlap spectrally.[39,48,49] By exploiting the differences in these absorption peaks, this study provided an effective approach of compensating atmospheric WV effect on 970-nm-based vegetation water indices. The approach leads to the development of a few indices that can provide robust estimation of vegetation CWC from satellite hyperspectral remote sensing data. This is important, since great uncertainty in surface reflectance retrievals can be induced through atmospheric correction due to inaccurate knowledge of atmospheric WV.[32] New 970-nm-based atmospherically resistant water indices are applied to Hyperion and GF5 hyperspectral images, and the results in Figs. 13 and 14 demonstrate the effectiveness of our approach in minimizing the uncertainties. This approach could also be applied to narrow-band multispectral cameras with suitable spectral configuration around the 970-nm water absorption feature. Future study will test the applicability of the developed water indices for FMC or EWT estimation.

4.2 Uncertainty in Parameterization of the New Water Indices

Stability of the correction coefficients in Eqs. (8)–(10) is very important for the application of the three new water indices in Eqs. (11)–(13). It may be affected by several factors including canopy reflectance, atmospheric correction, and sensor spectral configuration.

Both canopy and leaf parameters determine canopy reflectance.[50,51] Therefore, the PROSAIL coupled leaf-canopy reflectance model was used to assess the water indices with a range of canopy conditions described in Table 1. Our results show that variations of canopy and leaf parameters in Table 1 produced the parameterization result of the proposed 970-nm-based water indices with high R^2 (see Fig. 4). We did not consider the cases where target pixel is mixed with apparent water.

Impacts of atmospheric conditions, characterized by WV, AOT, aerosol type, imaging sun-canopy-sensor geometry, have also been considered using the 6S model simulations. Our results in Sec. 3.2 show that the error differences in WV used for atmospheric correction does not bring apparent variation in the correction coefficients in the proposed new water indices, whereas larger errors in AOT do. At AOT of 0.2, the normal error level of MODIS aerosol products (refer to Refs. 30 and 31) is $\pm(0.05 + 0.15 * AOT)$ and will only have very little effect on the parameterization results (see Fig. 7). Retrieval of aerosol from hyperspectral data such as Hyperion will be more accuracte than that from multispectral sensor such as MODIS.[52] Thus, incoporating AOT retrievals from hyperspectral data helps to ensure a more stable parameterization of the new water indices.

Parameterization of the proposed water indices is sensor-specific, dependent on spectral configurations, such as band position and spectral response function, thus, the specific k_λ values should be adapted from Fig. 4 for specific sensors, such as the Hyperion and the GF5 AHSI.

4.3 Limitations of New Atmospherically Resistant Water Indices in Improving Estimation of Vegetation Water Content

The ability for monitoring vegetation water status varies with different vegetation water indices. WI and NWIs are found to provide estimation of CWC with a higher accuracy than FMC and EWT.[2,13,14] NDWI is found to be inferior for CWC estimation than the 970-nm-based water indices,[13,53] which is consistent with our studies (see Fig. 12). The sensitivity of vegetation water indices to variations in vegetation water status is influenced by other canopy factors such as LAI, leaf angle distribution function, and mixed pixels.[41,50,51]

As shown in Fig. 15, the proposed water indices in this study are strongly correlated with their original water indices calculated using error-free reflectance data. Therefore, the new atmospherically resistant water indices would provide similar performance compared to their original 970-nm-based water indices calculated from error-free reflectance data in monitoring vegetation water status. Our results have showed that ARWI, NARWI-1, and NARWI-3 provide CWC estimation with an accuracy comparable with that provided by WI, NWI-1, and NWI-3 using field reflectance dataset (see Table 5 and Fig. 12).
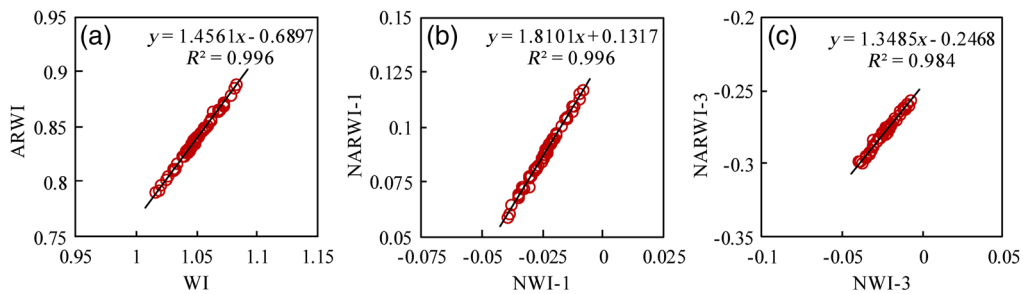
Fig. 15 Scatter plots of (a) WI vs. ARWI, (b) NWI-1 vs. NARWI-1, and (c) NWI-3 vs. NARWI-3 using field reflectance data obtained in Xiaotangshan, Beijing. The field reflectance data are considered having no atmospheric correction errors.

5 Conclusion

This study presented a simple method for reducing the impact of atmospheric correction errors on 970-nm-based vegetation water indices, e.g., WI, NWI-1, and NWI-3, by exploiting the differences in WV and liquid water absorption in this spectral region. We proposed atmospherically resistant version of the water indices, ARWI, NARWI-1, and NARWI-3. The proposed indices have been tested using simulated experimental data, winter wheat field data, as well as Hyperion and GF5 satellite hyperspectral data. The proposed indices are proven to be more resistant to atmospheric WV effect and can provide more accurate estimation of CWC than WI, NWI-1, and NWI-3, respectively. NWI-3 was the most affected by WV effect, and NARWI-3 provided the largest improvement in estimating CWC. Through adaptation, the proposed approach to developing the new 970-nm-based water indices could be applied in multispectral data with NIR water absorption peak. Further experiments are needed to assess the new indices using more satellite hyperspectral or narrow-band multispectral data covering different vegetation types.

Acknowledgments

References

1. G. Sepulcre-Cantó et al., "Monitoring yield and fruit quality parameters in open-canopy tree crops under water stress. Implications for ASTER," *Remote Sens. Environ.* **107**(3), 455–470 (2007).
2. G. Mendiguren et al., "Seasonal variation in grass water content estimated from proximal sensing and MODIS time series in a Mediterranean Fluxnet site," *Biogeosciences* **12**(18), 5523–5535 (2015).
3. P. J. Zarco-Tejada, C. A. Rueda, and S. L. Ustin, "Water content estimation in vegetation with MODIS reflectance data and model inversion methods," *Remote Sens. Environ.* **85**(1), 109–124 (2015).
4. T. Paz-Kagan and G. P. Asner, "Drivers of woody canopy water content responses to drought in a mediterranean-type ecosystem," *Ecol. Appl.* **27**(7), 2220–2233 (2017).
5. P. Ceccato et al., "Detecting vegetation leaf water content using reflectance in the optical domain," *Remote Sens. Environ.* **77**(1), 22–33 (2001).
6. E. R. Hunt and B. N. Rock, "Detection of changes in leaf water content using near- and middle-infrared reflectances," *Remote Sens. Environ.* **30**(1), 43–54 (1989).

7. F. M. Danson et al., "High-spectral resolution data for determining leaf water content," *Int. J. Remote Sens.* **13**(3), 461–470 (1992).

8. J. G. P. W. Clevers, L. Kooistra, and M. E. Schaepman, "Estimating canopy water content using hyperspectral remote sensing data," *Int. J. Appl. Earth Obs.* **12**(2), 119–125 (2010).

9. M. Yebra et al., "A global review of remote sensing of live fuel moisture content for fire danger assessment: moving towards operational products," *Remote Sens. Environ.* **136**, 455–468 (2013).

10. E. Neinavaz et al., "Retrieving vegetation canopy water content from hyperspectral thermal measurements," *Agric. For. Meteorol.* **247**, 365–375 (2017).

11. F. M. Danson and P. Bowyer, "Estimating live fuel moisture content from remotely sensed reflectance," *Remote Sens. Environ.* **92**(3), 309–321 (2004)

12. M. Yebra and E. Chuvieco, "Linking ecological information and radiative transfer models to estimate fuel moisture content in the Mediterranean region of Spain: solving the ill-posed inverse problem," *Remote Sens. Environ.* **113**(11), 2403–2411 (2009)

13. P. Ceccato et al., "Designing a spectral index to estimate vegetation water content from remote sensing data, Part 1, theoretical approach," *Remote Sens. Environ.* **82**(2), 188–197 (2002).

14. L. Liu, S. Zhang, and B. Zhang, "Evaluation of hyperspectral indices for retrieval of canopy equivalent water thickness and gravimetric water content," *J. Remote Sens.* **37**(14), 3384–3399 (2016).

15. G. L. Maire et al., "Calibration of a species-specific spectral vegetation index for leaf area index (LAI) monitoring: example with MODIS reflectance time-series on eucalyptus plantations," *Remote Sens.* **4**(12), 3766–3780 (2012).

16. J. Wu et al., "An exploratory analysis of spectral indices to estimate vegetation water content using sensitivity function," *Remote Sens. Lett.* **3**(2), 161–169 (2012).

17. B. C. Gao, "NDWI—a normalized difference water index for remote sensing of vegetation liquid water from space," *Remote Sens. Environ.* **58**(3), 257–266 (1996).

18. R. Fensholt and I. Sandholt, "Derivation of a shortwave infrared water stress index from MODIS near- and shortwave infrared data in a semiarid environment," *Remote Sens. Environ.* **87**(1), 111–121 (2003).

19. D. Y. Chen, J. F. Huang, and T. J. Jackson, "Vegetation water content estimation for corn and soybeans using spectral indices derived from MODIS near- and short-wave infrared bands," *Remote Sens. Environ.* **98**(2–3), 225–236 (2005).

20. M. Betty et al., "Mapping cropping practices of a sugarcane-based cropping system in Kenya using remote sensing," *Remote Sens.* **7**(11), 14428–14444 (2015).

21. J. Peñuelas et al., "Estimation of plant water concentration by the reflectance water index WI (R_{900}/R_{970})," *Int. J. Remote Sens.* **18**(13), 2869–2875 (1997).

22. D. A. Sims and J. A. Gamon, "Estimation of vegetation water content and photosynthetic tissue area from spectral reflectance: a comparison of indices based on liquid water and chlorophyll absorption features," *Remote Sens. Environ.* **84**(4), 526–537 (2003).

23. K. Chandrasekar et al., "Land surface water index (LSWI) response to rainfall and NDVI using the MODIS vegetation index product," *Int. J. Remote Sens.* **31**(15), 3987–4005 (2010).

24. M. A. Babar et al., "Spectral reflectance indices as a potential indirect selection criteria for wheat yield under irrigation," *Crop Sci.* **46**(2), 578–588 (2006).

25. B. Prasad et al., "Potential use of spectral reflectance indices as a selection tool for grain yield in winter wheat under great plains conditions," *Crop Sci.* **47**(4), 1426–1440 (2007).

26. M. Gutierrez, M. P. Reynolds, and A. R. Klatt, "Association of water spectral indices with plant and soil water relations in contrasting wheat genotypes," *J. Exp. Bot.* **61**(12), 3291–3303 (2010).

27. H. C. Claudio et al., "Monitoring drought effects on vegetation water content and fluxes in chaparral with the 970 nm water band index," *Remote Sens. Environ.* **103**(3), 304–311 (2006).

28. S. Sterckx et al., "The PROBA-V mission, image processing and calibration," *Int. J. Remote Sens.* **35**(7), 2565–2588 (2014).

29. T. Adão et al., "Hyperspectral imaging: a review on UAV-based sensors, data processing and applications for agriculture and forestry," *Remote Sens.* **9**(11), 1110 (2017).

30. L. A. Remer et al., "The MODIS aerosol algorithm, products and validation," *J. Atmos. Sci.* **62**(4), 947–973 (2005).
31. R. C. Levy et al., "Global evaluation of the collection 5 MODIS dark-target aerosol products over land," *Atmos. Chem. Phys.* **10**(21), 10399–10420 (2010).
32. J. Livingston et al., "Comparison of water vapor measurements by airborne Sun photometer and near-coincident *in situ* and satellite sensors during INTEX/ITCT 2004," *J. Geophys. Res. Atmos.* **112**, D12 (2007).
33. E. F. Vermote and M. N. Saleous, "Operational atmospheric correction of MODIS visible to middle infrared land surface data in the case of an infinite Lambertian target," in *Earth Science Satellite Remote Sensing*, J. J. Qu et al., Eds., pp. 123–153, Springer, Berlin, Heidelberg (2006).
34. R. Houborg and M. F. McCabe, "Impacts of dust aerosol and adjacency effects on the accuracy of Landsat 8 and RapidEye surface reflectances," *Remote Sens. Environ.* **194**, 127–145 (2017).
35. Y. J. Kaufman and D. Tanre, "Atmospherically resistant vegetation index (ARVI) for EOS-MODIS," *IEEE Trans. Geosci. Remote Sens.* **30**(2), 261–270 (1992).
36. A. R. Huete et al., "A comparison of vegetation indices over a global set of TM images for EOS-MODIS," *Remote Sens. Environ.* **59**(3), 440–451 (1997).
37. D. Wang et al., "A new neighboring pixels method for reducing aerosol effects on the NDVI images," *Remote Sens.* **8**(6), 489 (2016).
38. B. Sierk et al., "Field measurements of water vapor continuum absorption in the visible and near-infrared," *J. Geophys. Res. Atmos.* **109**, 657–678 (2004).
39. J. G. P. W. Clevers, L. Kooistra, and M. E. Schaepman, "Using spectral information from the NIR water absorption features for the retrieval of canopy water content," *Int. J. Appl. Earth Obs.* **10**(3), 388–397 (2008).
40. L. Liu et al., "Detection of leaf and canopy EWT by calculating REWT from reflectance spectra," *Int. J. Remote Sens.* **31**(10), 2681–2695 (2010).
41. P. J. Zarco-Tejada, C. A. Rueda, and S. L. Ustin, "Water content estimation in vegetation with MODIS reflectance data and model inversion methods," *Remote Sens. Environ.* **85**(1), 109–124 (2003).
42. Y. Liu, "Visible-shortwave infrared hyperspectral imager of GF-5 satellite," *Spacecr. Recovery Remote Sens.* **39**(3), 25–28 (2018).
43. G. P. Anderson et al., "MODTRAN4-based atmospheric correction algorithm: FLAASH (fast line-of-sight atmospheric analysis of spectral hypercubes)," *Proc. SPIE* **4725**, 65–71 (2002).
44. S. Jacquemoud and F. Baret, "Prospect: a model of leaf optical properties spectra," *Remote Sens. Environ.* **34**(2), 75–91 (1990).
45. W. Verhoef, "Light scattering by leaf layers with application to canopy reflectance modelling: the SAIL model," *Remote Sens. Environ.* **16**(2), 125–141 (1984).
46. E. F. Vermote et al., "Second simulation of the satellite signal in the solar spectrum (6S), 6S User Guide Version 3," 2006, http://6s.ltdri.org.
47. "HITRAN on the Web," Harvard-Smithsonian Center for Astrophysics (CFA), Cambridge, MA, USA, and V.E. Zuev Institute of Atmospheric Optics (IAO), Tomsk, Russia, http://hitran.iao.ru.
48. B. C. Gao and A. F. H. Goetz, "Column atmospheric water vapor and vegetation liquid water retrievals from airborne imaging spectrometer data," *J. Geophys. Res. Atmos.* **95** (D4), 3549–3564 (1990).
49. R. Pu et al., "Spectral absorption features as indicators of water status in coast live oak (*quercus agrifolia*) leaves," *Int. J. Remote Sens.* **24**(9), 1799–1810 (2003).
50. L. Serrano et al., "Deriving water content of chaparral vegetation from AVIRIS data," *Remote Sens. Environ.* **74**(3), 570–581 (2000).
51. Y. Xiao et al., "Sensitivity analysis of vegetation reflectance to biochemical and biophysical variables at leaf, canopy, and regional scales," *IEEE Trans. Geosci. Remote Sens.* **52**(7), 4014–4024 (2014).
52. T. Perkins et al., "Retrieval of atmospheric properties from hyper and multispectral imagery with the FLAASH atmospheric correction algorithm," *Proc. SPIE* **5979**, 59790E (2005).

53. M. Vohland, "Using imaging and non-imaging spectroradiometer data for the remote detection of vegetation water content," *J. Appl. Remote Sens.* **2**(1), 023520 (2008).

Quanjun Jiao is an associate professor at the Aerospace Information Research Institute, Chinese Academy of Sciences. He received his bachelor's degree in cartography and geographical information systems from the Peking University in 2003 and his PhD in cartography and geographical information system from the Institute of Remote Sensing Applications, Chinese Academy of Sciences, in 2008. His research interest is in application of vegetation remote sensing.

Liangyun Liu is a professor at the Aerospace Information Research Institute, Chinese Academy of Sciences. He received his PhD from Xi'an Institute of Optics and Precession Mechanics, Chinese Academy of Sciences, in 2000. He was honored by the National Science Fund for Outstanding Young Scholars in 2018. His research interest is in vegetation quantitative remote sensing.

Jiangui Liu is currently a physical scientist with the Science and Technology Branch, Agriculture and Agri-Food Canada. He received his bachelor's degree in electronics engineering from Tsinghua University in 1990 and his PhD in cartography and remote sensing from the Chinese Academy of Sciences in 1999. His research interests include remote sensing for crop and soil biophysical parameter estimation, crop productivity, and agri-environmental sustainability assessment.

Hao Zhang is an associate professor at the Aerospace Information Research Institute, Chinese Academy of Sciences. He received his PhD in cartography and geographical information systems from the Institute of Remote Sensing Applications, Chinese Academy of Sciences, in 2009. His research interest is in atmospheric correction of remote sensing data.

Bing Zhang is a professor at the Aerospace Information Research Institute, Chinese Academy of Sciences. He received his PhD in cartography and geographical information systems, from the Institute of Remote Sensing and Digital Earth, Chinese Academy of Sciences, in 2003. He was honored by the National Science Fund for Outstanding Young Scholars in 2013. His research interest is in hyperspectral remote sensing.